CrossMark

ARTICLE

Influence of solid solution strengthening on the local mechanical properties of single crystal and ultrafine-grained binary Cu–Al*X* solid solutions

Verena Maier-Kiener
Montanuniversität Leoben, Department Physical Metallurgy and Materials Testing, Leoben A-8700, Austria

Xianghai An
Shenyang National Laboratory for Materials Science, Institute of Metal Research, Chinese Academy of Sciences, Shenyang 110016, People's Republic of China; and School of Aerospace, Mechanical and Mechatronic Engineering, The University of Sydney, Sydney, NSW 2006, Australia

Linlin Li and Zhefeng Zhang
Shenyang National Laboratory for Materials Science, Institute of Metal Research, Chinese Academy of Sciences, Shenyang 110016, People's Republic of China

Reinhard Pippan
Austrian Academy of Sciences, Erich-Schmid-Institute of Materials Science, Leoben A-8700, Austria

Karsten Durst[a)]
TU Darmstadt, Physical Metallurgy, Darmstadt 64287, Germany

(Received 23 May 2017; accepted 14 July 2017)

In this work, the influence of Al-solutes on the mechanical behavior of Cu–Al*X* solid solutions has been studied using indentation strain rate jump tests for single crystalline and ultrafine-grained (UFG) microstructures from high pressure torsion (HPT) processing. Al-solutes in Cu classically lead to a solid solution strengthening, coupled with a decrease in stacking fault energy, which influences also the grain size after HPT processing. For all alloys, a higher hardness is found at lower indentation depths, which can be nicely described by a modified Nix/Gao model down to 100 nm indentation depth. Among the single crystals, the largest size effects are found for the higher solute contents, indicating a stronger work hardening at small length scales for the solid solutions. The dilute UFG solid solutions showed a strong softening after a strain rate reduction test, with a pronounced transient region. Cu–Al15 is, however, quite stable, showing abrupt changes in hardness without strong transients. This indicates that solute solution strengthening does not only influence the indentation size effect and structure formation during HPT processing but also stabilizes the grain structure during subsequent deformation.

I. INTRODUCTION

The deformation mechanism in single crystalline (SX) and ultrafine grained face-centered cubic (FCC) solid solutions have gained much attention in the last decade and particularly, nanoindentation has been used to study different size effects in their mechanical behavior.[1] Specifically for ultrafine-grained (UFG) materials, besides the increasing strength, in some cases also the tensile ductility can be increased.[2] This paradoxon was already widely investigated in research over the last decade, but it is not fully understood yet.[3,4] One important aspect seems to be the enhanced strain rate sensitivity (SRS) of UFG microstructures, which relates to dislocation storage and annihilation mechanism at grain boundaries.[4–6]

Dislocation storage mechanisms also play an important role during nanoindentation. Specifically for indentation testing of soft annealed single crystals, an increasing hardness is found for smaller indentation depths, referred to as the indentation size effect (ISE).[7] Strain gradients are introduced into the material, which are believed to cause the additional strengthening at small length scales.[8–10] For solid solutions, stronger size effects and hardness increases have been found compared to unalloyed pure metals. This effect is not fully understood, but has been attributed to an increased work hardening of the alloys and higher frictional stresses due to solid solution strengthening.[11] Nanoindentation can also be used to assess the strengthening mechanism in nanocrystalline (NC) or UFG metals. Refining the microstructure down to the NC regime by severe plastic deformation leads to an increased hardness, coupled with

Contributing Editor: Mathias Göken
[a)]Address all correspondence to this author.
e-mail: k.durst@phm.tu-darmstadt.de
DOI: 10.1557/jmr.2017.320

https://doi.org/10.1557/jmr.2017.320 Published online by Cambridge University Press

 © Materials Research Society 2017

a strong reduction of the size effect.[1] During indentation of UFG/NC-material, often many hundreds or thousands of grains are deformed within the plastic zone, making it possible to observe Hall–Petch and Taylor strengthening. Furthermore, an enhanced SRS, often found during macroscopic uniaxial testing, also influences the indentation hardness.[12,13]

In this work, different Cu and Cu–Al*X* solute solutions were investigated regarding the influence of stacking fault energy (SFE) and solute solution content on the small scale deformation behavior such as ISE and thermally activated deformations processes in terms of SRS and activation volume. Highly deformed microstructures in the UFG and NC regime [in the following referred as UFG and high pressure torsion (HPT)-deformed] were produced by HPT[14,15] and SX and UFG deformation behavior is set into context. The work was also motivated by several studies, where the influence of solid solution strengthening and SFE on the structure formation during severe plastic deformation was investigated. One might argue that due to different SFEs and thus different dislocation movement and interaction, also the grain size might be affected.[16–22]

Furthermore, it has been shown that depending on SFE and the Holomon–Zener parameter, twinning will become an acting deformation mechanism.[23,24] According to that HPT-deformed should still deform by dislocation motion; while for Cu–Al15, twinning becomes more important.

Of course, the SFE influences the grain refinement itself; however, it was also already pointed out that the solute content and the homologous deformation temperature are more influencing the saturation grain size and the resultant microstructure.[24,25] Currently, there is still an open debate on the exact mechanism leading to grain refinement in solid solutions, considering both the influence of SFE and the mobility of grain boundaries due to solute effects.

II. EXPERIMENTAL

The experiments were conducted on SX and UFG Cu and Cu-Al*X* at.% alloys using Cu of 99.9999% purity with a SFE of 45 mJ/m^2 and four Cu–Al*X* alloys with medium and low SFEs (see Table I). SX Cu–Al*X* alloys were processed by the Bridgman process.

HPT was conducted in an up-scaled HPT device[26] at room temperature (RT) under quasiconstrained conditions using disks with a diameter of 30 mm and thicknesses of 2.5 mm.[27] These disks were processed by HPT through 5 revolutions with a speed of 0.06 rpm under an imposed pressure of 5.0 GPa. For further mechanical testing, samples were taken out of the outer regions of the HPT disks, where a saturated grain size regime was assumed.

TABLE I. SFE and grain size of the investigated materials.

	SFE[16,27–29] [mJ/m^2]	Grain diameter[27] [nm]
Cu	~45	~140
Cu–Al5	~28	~65
Cu–Al8	~17	-
Cu–Al15	~6	~40
Cu–Al16	~6	-

For all microstructural and alloying conditions, cross sections were prepared for metallographic examinations and nanoindentation testing. The specimens were ground, then polished with a diamond slurry down to 1 μm, and finally, electrolytically polished. Examination of the grain structures as well as characterization of the deformation structures underneath a residual indentation were performed using FIB-SEM (Zeiss, Oberkochen, Germany) in BSE (Back scattered electrons) mode. The grain size was evaluated using the line intersection method on SEM micrographs, where a distinction between high-angle and low-angle boundaries was not made.

Nanoindentation experiments were performed with a Nanoindenter G200 (Keysight Tec., Santa Rosa, CA) equipped with a continuous stiffness measurement (CSM) unit and a three-sided Berkovich diamond pyramid. Machine stiffness and tip shape calibration was performed according to the Oliver–Pharr[30] method, and nanoindentation testing was carried out at RT (22 °C). For analysis of the ISE, constant loading rate (load controlled—LC) nanoindentation experiments up to 500 mN were performed. By applying a constant loading time of 15 s and 7–10 loading/unloading cycles, a constant corresponding indentation strain rate at the point of maximal load of 0.033 s^{-1} was provided for all cycles.[31]

For strain rate controlled experiments, the CSM frequency was set to 40 Hz and a harmonic amplitude of 3 nm was superimposed. According to Durst et al.,[11] Pharr et al.,[32] and Merle et al.,[33] the CSM technique can lead to a significant error in the indentation data for soft metallic materials like single crystals with a large E/H ratio (for SX-Cu ~240, for UFG-Cu ~50). This error is directly related to the dynamic unloading of the tip and influences the measured force, displacement, and stiffness data. Therefore, Pharr et al.[32] suggested a correction for load and displacement which considers the harmonic load and harmonic displacement in the load–displacement data, which is implemented in any current software version and has been used in the current approach.

The local SRS was investigated using nanoindentation strain rate jump tests.[12] The interested reader may refer to a recent overview on dynamic indentation testing by Durst and Maier for further details on the testing procedure and important testing issues during transient nanoindentation testing.[31] Generally, the indentation

https://doi.org/10.1557/jmr.2017.320 Published online by Cambridge University Press

strain rate $\dot{P}/P$ was initially held constant (P: indentation load, 0.05 s^{-1} equivalent to macroscopic strain rate of 0.025 s^{-1})[34] until an indentation depth of 500 nm was reached, ensuring a constant microstructure underneath the indenter tip for the UFG-samples. Afterward, strain rate jumps to 0.0025 ($\dot{\varepsilon}_{ind}$ = 0.005 s^{-1}) and 0.0005 s^{-1} ($\dot{\varepsilon}_{ind}$ = 0.001 s^{-1}), respectively, were applied every 500 nm up to a maximum indentation depth of 2500 nm in a repetitive manner. The strain rate dependent hardness H was determined instantaneously, directly from the hardness data before and after each jump.[31,35] For quantifying the dominating deformation processes, the local SRS $m = \partial \ln H / \partial \ln \dot{\varepsilon}$ and an apparent activation volume $V^* = C^* \cdot \sqrt{3} \cdot k_B \cdot T/mH$ were evaluated directly from the resulting hardness H differences depending on the applied strain rate $\dot{\varepsilon}$ (with C^*: Constraint factor of 2.8, k_B: Boltzmann constant, T: RT 295 K).[36]

III. RESULTS & DISCUSSION

Previous to the size effect investigations and the characterization of the dominating thermally activated processes, the hardness and Young's modulus of all samples were characterized by constant strain rate (0.05 s^{-1}) nanoindentations (Table II).

With increasing alloying content, the hardness for both SX and UFG condition increases. The Young's modulus for the HPT-deformed alloy is overall higher because the SX condition was tested in the weak ⟨100⟩-orientation. Further deeper aspects in the deformation behavior will be addressed within the next section.

A. Indentation size effect

Figure 1 displays the results from the LC indentation test on both HPT- and SX-samples up to 500 mN maximum load. As expected, the SX-alloys exhibit a much smaller bulk hardness, but show a stronger increase in hardness with decreasing depth. For comparison reasons, the hardness versus contact depth data are plotted linearly [Fig. 1(a)]. In the linear plot in Fig. 1(a), a nearly constant hardness at large indentation depths is observed for all microstructural conditions, with a much stronger hardness increase at small depths for the SX alloys.

For the further analysis of the depth dependency of hardness, the data were analyzed according to the well-known Nix–Gao model,[7] where a macroscopic depth independent hardness H_0 is considered. The model thus describes the size effect based on a size-independent strength level of the material, in which all strengthening contributions are included.

$$\frac{H}{H_0} = \sqrt{1 + \frac{h^*}{h}} \quad , \tag{1}$$

Here, H is the depth dependent hardness at a given indentation depth h, H_0 corresponds to the macroscopic hardness, and h^* represents an internal indentation length scale, which describes the depth dependency of the hardness and the extent of the ISE. It is evident that the hardness data down to a depth of 100 nm can be described nicely by the Nix–Gao analysis, yielding in a constant characteristic indentation length scale h^* for

TABLE II. Mechanical properties of SX-Cu–AlX in ⟨100⟩ orientation and of UFG HPT-deformed Cu–AlX determined by constant strain rate indentation to 2000 nm indentation (averaging region: 1800–1900 nm) —ISE not considered yet.

Alloy	Hardness [GPa]	Young's modulus [GPa]
SX Cu	0.64 ± 0.01	114.0 ± 1.2
SX Cu–Al8	0.85 ± 0.01	115.2 ± 1.1
SX Cu–Al16	1.19 ± 0.01	122.3 ± 2.3
UFG Cu	1.6 ± 0.06	138.2 ± 2.5
UFG Cu–Al5	2.64 ± 0.07	131.4 ± 1.9
UFG Cu–Al15	2.81 ± 0.2	124.5 ± 5.1

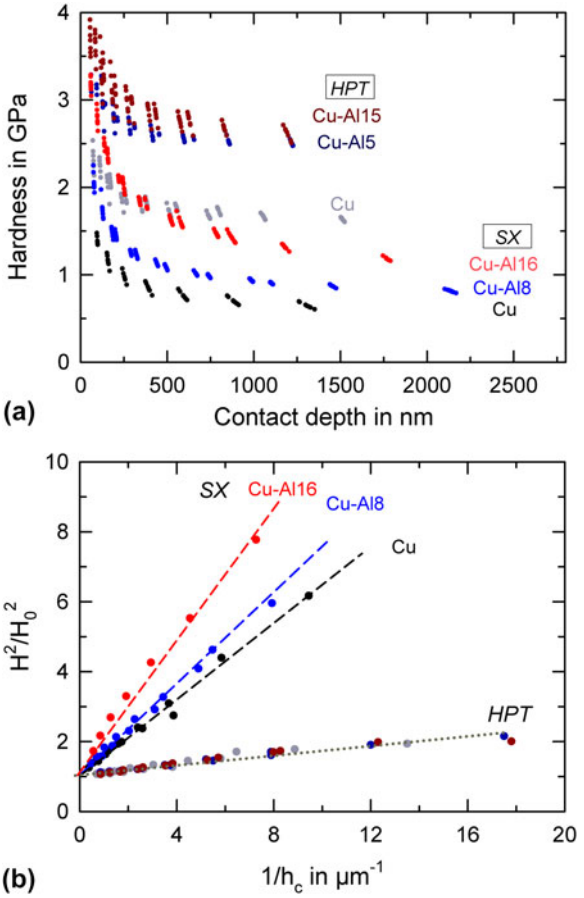


FIG. 1. LC nanoindentation experiments—ISE; hardness in SX- and HPT-Cu and Cu–AlX solid solutions: (a) Hardness versus contact depth and (b) Nix–Gao analysis.

https://doi.org/10.1557/jmr.2017.320 Published online by Cambridge University Press

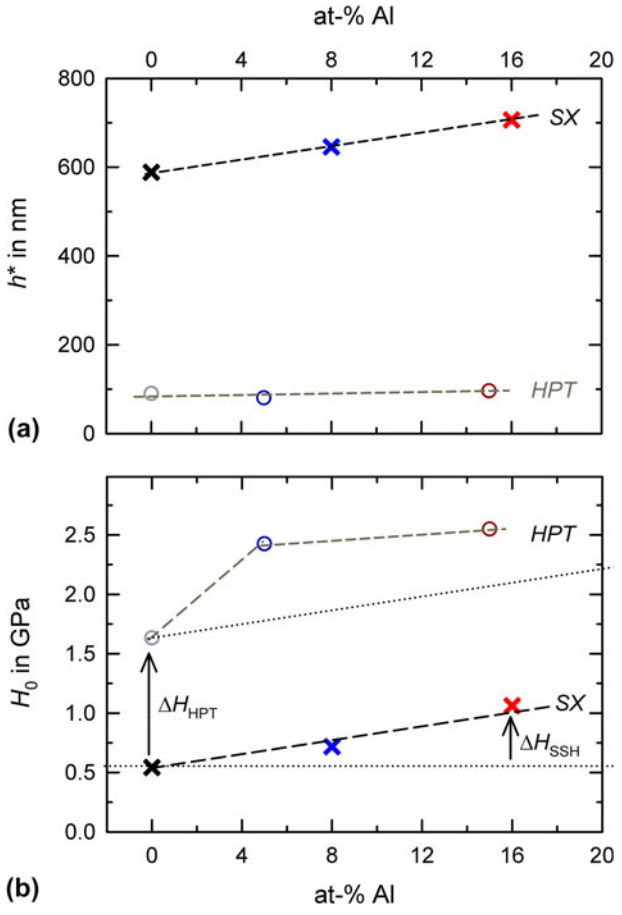


FIG. 2. Analysis of the ISE according to Nix–Gao in relationship to Al content (SSH contribution) for SX-state and HPT-deformed UFG state (HPT contribution), (a) internal indentation length scale, and (b) macroscopic hardness versus Al content.

each alloy [Fig. 1(b)]. Even though each UFG HPT-deformed alloy exhibits a different macroscopic hardness, all data in the Nix–Gao analysis collapses on the same master curve with hardly any dependency of the size effect on the alloying content. Overall, this indentation behavior can be described by a characteristic internal indentation length scale $h^* \sim 100$ nm, nearly independent of the alloying content [Fig. 2(a)].

The SX-alloys, however, show a clear dependency of the hardness increase on the alloy content. The Cu–Al16 alloy exhibits the highest hardness coupled with the strongest size effect, which is indicated in the largest characteristic indentation length scale of $h^* \sim 700$ nm. For discussing the higher strength at smaller length scales of the SX-solid solutions, the dislocation model of the ISE needs to be considered. Nix and Gao[7] discuss the hardness increase based on geometrically necessary dislocations (GNDs). The total dislocation line length necessary to form the residual impression depends on the indenter opening angle. A dependency of the hardness on the solute content requires thereby a higher dislocation density within the plastically deformed volume for the alloys in comparison to the unalloyed crystals. One reason for higher dislocation densities in the plastic zone could be a reduction in the effective storage volume for GNDs, as being discussed by Durst et al.[37] Based on the modification to the Nix–Gao model presented in that work, the storage volume for GNDs is estimated. It is clear that the solute content with the reduced SFE and higher solid solution strengthening will hinder dislocation rearrangements below the indenter. This might also cause a stronger work hardening in the highly stressed region below the indent, causing the increased size effect. Further experiments trying to quantify the dislocation content, distribution, and character in terms of full and partial dislocations as well as twins below the indenter are required to further elucidate the mechanism. Rester et al.[38] already showed successfully by an approach where they combined nanoindentation and electron back scatter diffraction (EBSD) of several FCC-materials with different SFEs that the SFE does not significantly influence the ISE. They also found for the metal with the lowest SFE (Ag) the largest size effect,[38,39] but the overall deformation structure underneath all indentations in the different SFE-materials rather seemed to be alike, with little indication of twinning activity.

From the macroscopic hardness data, it is also possible to discuss the relative contributions of solid solution and Hall–Petch strengthening for the HPT-deformed alloys [Fig. 2(b)]. The contribution of solid solution strengthening is assessed by comparing the macroscopic hardness of Cu to the hardness of the alloyed samples: $H_{\text{solid solution}} = H_{\text{alloy}} - H_{\text{unalloyed}}$. Taking the hardness of the UFG HPT Cu sample, the hardness of the HPT solid solution solid is now estimated by simply adding the solid solution contribution $H_{\text{HPTalloy}} = H_{\text{HPTCu}} + H_{\text{solid solution}}$ (Fig. 2, dotted line). Solid solution strengthening by itself can therefore not explain the increased strength of the HPT alloys, but in addition, it is necessary to consider the grain size and the enhanced solid solution strengthening on the strength evolution in the alloys after HPT processing.

The strong ISEs observed during indentation testing resemble the stronger structural refinement and higher defect densities after HPT processing, even though the deformation processes are quite different. The hardness at small depth of the Cu–16Al single crystal is in the range of 3.2 GPa, which is even higher compared to the macroscopic hardness of the HPT-deformed UFG-sample. It should be noted that the hardness value determined at a depth of 100 nm stems from a much larger depth as the pop-in (elastic–plastic transition) occurred; thus, the plastically deformed zone is already fully evolved. Clearly, the SX-states exhibit a strong work hardening in the plastically deformed volume, which for Cu16Al leads to even higher deformation resistance in comparison to the HPT-alloy.

https://doi.org/10.1557/jmr.2017.320 Published online by Cambridge University Press

B. Strain rate sensitivity

Figure 3 shows the load displacement data of the different alloys and microstructures tested using the nanoindentation strain rate jump method. For the SX-materials [Fig. 3 (a—left side)], only slight variations in the load displacement curves are found after each strain rate jump indicating negligible SRS. For SX-Cu–Al16 pronounced serrations within the loading curve are observed, which might be related to serrated yielding and dynamic strain aging effects according to Portevin-le-Chatelier (PLC)[40] in this SX alloy. The serrations in the load displacement curve lead also to pronounced serrations in the hardness, with a slightly negative SRS and increasing hardness with decreasing strain rates. Due to the serrations, no attempt was made to enumerate the SRS exponent. The PLC effect is found in many solid solutions in a well-defined parameter window depending on alloying content, diffusivity, applied strain rate, and deformation temperature. The dynamic strain aging between the Cottrell-like solute cloud and the moving dislocation leads to load drop and the mentioned serrated yielding behavior. For Cu and Cu–Al5, the hardness is nearly independent of the applied strain rate within the parameters used in this study, as seen in the load displacement curves and expected for FCC-metals according to literature. The SX-alloys exhibit also a strong ISE, in detail described in the chapter before.

For the UFG-alloys, the load level for the same indentation depth is much higher and significant changes in the shape of the load displacement curves are observed after each strain rate jump. The corresponding hardness curves are clearly affected by the applied strain rate changes, leading to a reduction in hardness for lower strain rates, indicating an enhanced SRS for all Cu-alloys. Interestingly, no further serrations in the hardness data are found for Cu–Al15, although SX-Cu–Al16 exhibited a strong PLC effect. This could be caused by the higher stresses in the UFG-condition and thus the overall changed dislocation velocities. Furthermore and in good accordance with the previously discussed LC indentations, only a slight hardness increase is found for HPT-Cu–Al15 compared to HPT-Cu–Al5. HPT-Cu and HPT-Cu–Al5 show during strain rate reduction a transient behavior, followed by an appreciable softening, whereas the hardness of HPT-Cu–Al15 changes quickly and remains fairly constant after strain rate changes. HPT-Cu and HPT-Cu–Al5 seem to strain soften indicated by lines in Fig. 3, which is indicative of a nonsteady state microstructure and i.e., grain coarsening, assisted by large deformation due to indentation.

To examine the possibility of deformation-induced grain growth, Fig. 4 shows FIB cross sections of strain rate jump indentations in the HPT-deformed alloys. It is found that the grain size within the plastically deformed

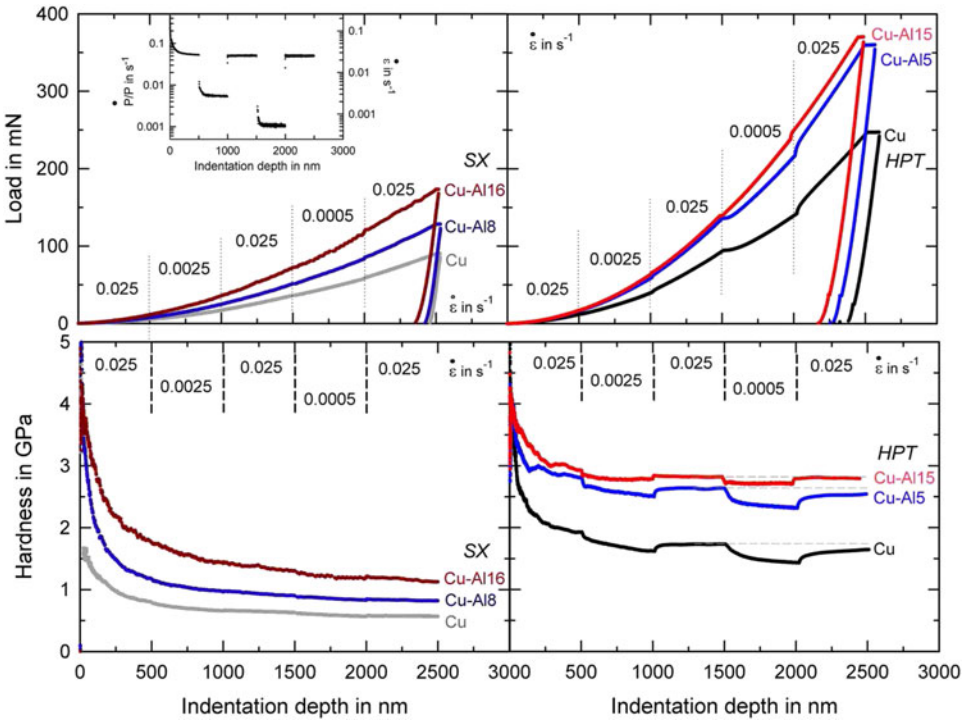


FIG. 3. Load–displacement data and hardness versus indentation depth curves for Cu–Al*X* from nanoindentation strain rate jump tests by applying the displayed loading/strain rate scheme in the top left diagram (left side) SX-states and (right side) UFG HPT-deformed states. Dashed lines in HPT condition indicates strain softening for Cu and Cu–Al5 in HPT state.

https://doi.org/10.1557/jmr.2017.320 Published online by Cambridge University Press

zone of the Cu and Cu–Al5 alloy has slightly increased, while the grain size in Cu–Al15 remains fairly stable. Moreover, we did not observe any twinning within the plastic zone.

For further clarification, a magnified detail of the transient of the strain rate jump is shown for all alloys and microstructures in Fig. 5(a), illustrating the described cases from no-SRS and PLC behavior for the SX-conditions to pronounced transients for HPT-Cu and HPT-Cu–Al5 and a quite abrupt change in hardness for Cu–Al16, which will be discussed later on. In Fig. 5(b), the instantaneous SRS and corresponding activation volumes V^* are plotted, both taken instantaneously from the hardness data directly at each applied strain rate jump. While this is a common procedure, it should be kept in mind that the values reported here have been evaluated for an unstable microstructure and not for a constant microstructure typically assumed in such transient experiments.

Interestingly, HPT-Cu, with the lowest hardness and the largest grain size, exhibits the largest strain rate exponent of $m = 0.029$. UFG-Cu–Al15, with the highest strength and the smallest grain size has the smallest SRS $m = 0.010$. Thus, it is obvious that not only the apparent grain size in FCC-materials governs the thermally activated processes, but also the alloying content itself has to be majorly taken into account. In literature, annihilation of dislocations at grain boundaries has been discussed as

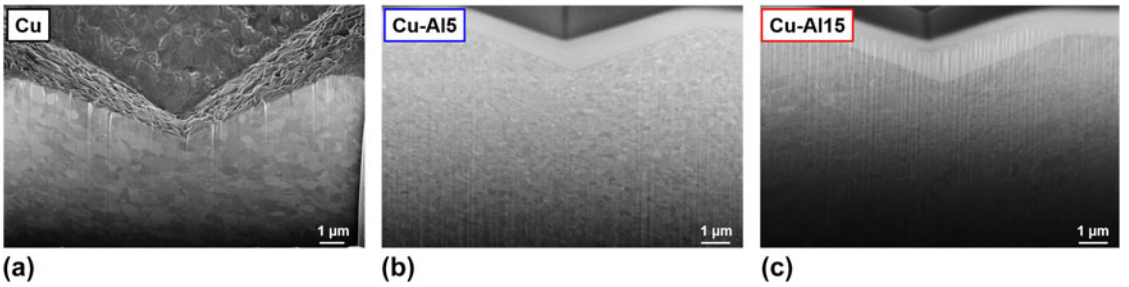


FIG. 4. FIB cross sections after strain rate jump controlled indentation experiments, (a) UFG-Cu, (b) UFG-Cu–Al5, (c) UFG-Cu–Al15.

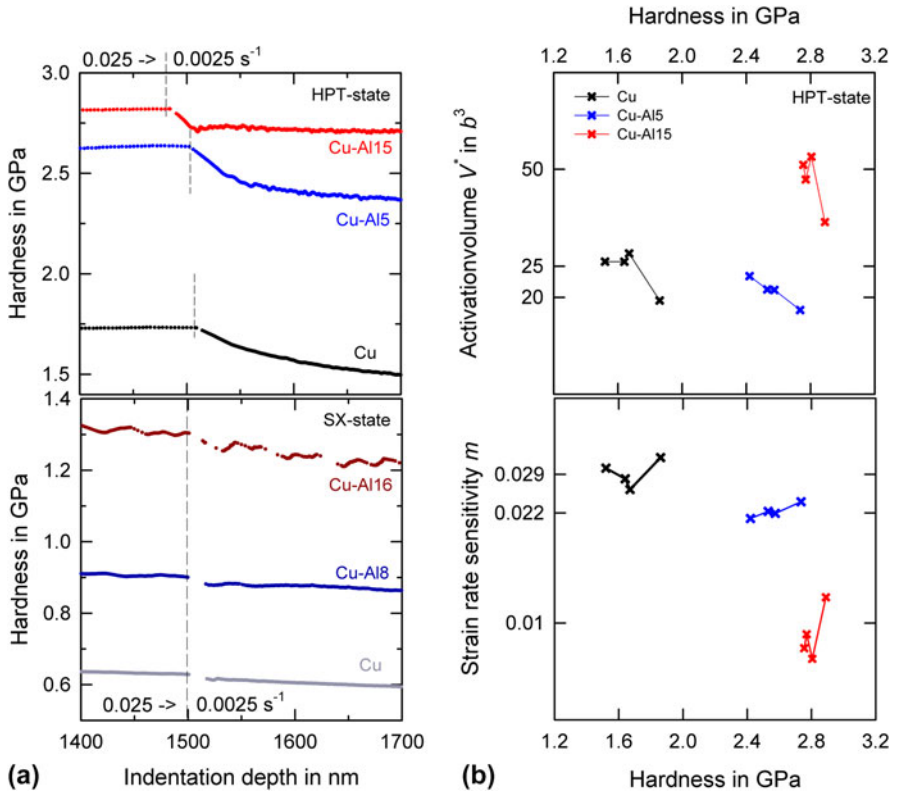


FIG. 5. (a) Magnification of single strain rate jumps for UFG HPT-(upper part) and SX-(lower part) conditions, and (b) corresponding SRS m and activation volume V^* versus H for UFG Cu and Cu–AlX solid solutions.

https://doi.org/10.1557/jmr.2017.320 Published online by Cambridge University Press

one possible mechanism for the enhanced SRS of UFG materials, leading to a reduction of dislocation content at smaller strain rates.[41] There has been indications by dislocation dynamics and diffusion kinetics simulations, that indeed dislocation annihilation due to climb of dislocations within the grain boundaries can yield enhanced SRS.[42] For all these cases, however, a smaller grain size at the same homologous temperature should yield a higher SRS, which we do not observe for UFG-CuAl15. At that point, the main question arises, to which extend the solid solution is contributing to the SRS. Of course, the different SFEs are influencing the dislocation mobility and motion as well as the resulting dislocation structure. However, does that influence the thermally activated processes as well?

For that reason, the data shown here has to be carefully considered. It is true that both Cu and Cu–Al5 show unstable microstructures during nanoindentation testing. The strain rate changes themselves are affected by a pronounced, but very smooth transient behavior after each jump independent of the magnitude and sign of the rate change. Within this transient zone, the hardness changes slowly to a new strain rate dependent hardness level. This was also proven by FIB cross sections (Fig. 4). Moreover, the SRS for both samples is increased to values around 0.03, paired with very low V^* of around $20 \cdot b^3$ indicating similar dominating deformation mechanisms. The value of the latter parameter agrees well with the literature.[43] Clearly, the SRS values and apparent activation values reported here are due to several overlapping mechanism acting in an unstable microstructure. A similar behavior has been also observed for UFG-Cu after compression testing at elevated temperatures, with coarsening contributing to the SRS.[44]

For HPT Cu–Al15, the governing deformation behavior obviously changes and also a more stable microstructure was observed underneath the indenter in the plastically deformed regions. HPT-Cu–Al15 does not show any pronounced transient behavior after the strain rate jump, but rather a very distinct, immediate hardness change is observed. This indicates that the microstructure seems to be much more stable and thus a constant strain rate dependent steady-state hardness level can be reached. At the same time, the calculated SRS decreases, which can be also contributed to the higher hardness level due to the higher solid solution strengthening.

Thus, besides grain size also solid solution strengthening is contributing to the time dependent properties of the Cu–Al*X* alloys. It is well known in literature, that dynamic strain aging can control the movement of dislocations to a large extent. The dislocation velocities are controlled by the diffusing solute cloud around the dislocation core and therefore depending on temperature and applied stress level, the strain rate, the dislocation motion is greatly impeded. The reduced SFE together with the increased solid solution strengthening changes the grain boundary migration characteristics and minimizes the interaction as well as possible annihilation processes of the dislocations within the grain boundary. This also leads to a more stable microstructure and a reduced SRS of HPT-Cu–Al15. At this point, we cannot rule out local ordering or enrichment of Al in the grain boundaries as another factor influencing the grain boundary mobility as well as the dislocation grain–boundary interaction. Interestingly, the solid solution strengthening is also contributing to the grain refinement and saturation grain size after HPT processing,[19,23,24,27] which is mimicked here by the lower SRS of the alloy, despite its smaller grain size.

IV. CONCLUSIONS & OUTLOOK

In this work, the influence of Al-solutes on the mechanical behavior of Cu–Al*X* solid solutions has been studied using indentation strain rate jump tests for SX and UFG microstructures from HPT processing. Al-solutes in Cu classically lead to a solid solution strengthening, coupled with a decrease of the SFE.

Concerning the indentation behavior and size effects, the well-known behavior is found, namely that fine grained materials exhibit a much smaller ISE and that both material conditions are well described by the Nix/Gao model down to indentation depths of 100 nm. Furthermore, a much stronger size effect is observed for the solid solutions, indicating that dislocation mechanism leads to a higher dislocation content at the same depth for the solid solutions. The hardness of the SX Cu–Al16 at 100 nm indentation depth is nearly as high as the hardness of the UFG material, which is quite remarkable. The solid solution strengthening contribution is clearly depicted for the macroscopic hardness data of the single crystals. However, additional refinement of the microstructure needs to be considered when comparing the UFG solid solution conditions. At large indentation depths, Cu and Cu–Al5 show significant softening, which can be attributed to a coarsening of the grain structure below the indent. The smaller hardness of the dilute solid solutions is therefore partly due to recovery process at grain boundaries. The apparent SRS of the dilute solid solutions is moreover relatively high, which is partly also attributed to the coarsening of the grain structure. Cu–Al15 is however quite stable and the observed SRS is related to the fine grain size. The higher solute content with the stronger solid solution strengthening and reduced SFE seems to be not only important for the minimum grain size after HPT, but also could explain the more stable microstructure with a comparatively small SRS.

ACKNOWLEDGMENTS

Parts of the experimental work were performed when V.M-K. and K.D. were still at the Chair of General

https://doi.org/10.1557/jmr.2017.320 Published online by Cambridge University Press

Materials Properties (FAU Erlangen-Nürnberg); therefore, the authors thank Prof. M. Göken for his support. Further, financial support by the Austrian Federal Government (837900) within the framework of the COMET Funding Program (MPPE, A7.19) (V.M-K.) and by the ERC (USMS: 340185) (R.P.) as well as the National Natural Science Foundation of China (NSFC) under grant Nos. 51331007 and 51471170 (Z.F.) is highly appreciated.

REFERENCES

1. B. Backes, K. Durst, and M. Göken: Determination of plastic properties of polycrystalline metallic materials by nanoindentation: Experiments and finite element simulations. *Philos. Mag.* **86**, 5541 (2006).
2. R.Z. Valiev, I.V. Alexandrov, Y.T. Zhu, and T.C. Lowe: Paradoxon of strength and ductility in metals processed by SPD. *J. Mater. Res.* **17**, 5 (2002).
3. H.W. Höppel, J. May, and M. Göken: Enhanced strength and ductility in ultrafine-grained aluminium produced by accumulative roll bonding. *Adv. Eng. Mater.* **6**, 781 (2004).
4. J. May, H.W. Höppel, and M. Göken: Strain rate sensitivity of ultrafine-grained aluminium processed by severe plastic deformation. *Scr. Mater.* **53**, 189 (2005).
5. J. May, H.W. Höppel, and M. Göken: Strain rate sensitivity of ultrafine grained fcc- and bcc-type metals. *Mater. Sci. Forum* **503–504**, 781 (2006).
6. Y.J. Li, J. Mueller, H.W. Höppel, M. Göken, and W. Blum: Deformation kinetics of nanocrystalline nickel. *Acta Mater.* **55**, 5708 (2007).
7. W.D. Nix and H. Gao: Indentation size effects in crystalline materials: A law for strain gradient plasticity. *J. Mech. Phys. Solids* **46**, 411 (1998).
8. B. Backes, Y.Y. Huang, M. Göken, and K. Durst: The correlation between the internal material length scale and the microstructure in nanoindentation experiments and simulations using the conventional mechanism-based strain gradient plasticity theory. *J. Mater. Res.* **24**, 1197 (2009).
9. D. Kiener, K. Durst, M. Rester, and A.M. Minor: Revealing deformation mechanisms with nanoindentation. *JOM* **61**, 14 (2009).
10. M.A. Lodes, A. Hartmaier, M. Göken, and K. Durst: Influence of dislocation density on the pop-in behavior and indentation size effect in CaF_2 single crystals: Experiments and molecular dynamics simulations. *Acta Mater.* **59** (2011).
11. K. Durst, O. Franke, A. Böhner, and M. Göken: Indentation size effect in Ni–Fe solid solutions. *Acta Mater.* **55**, 6825 (2007).
12. V. Maier, K. Durst, J. Mueller, B. Backes, H.W. Höppel, and M. Göken: Nanoindentation strain-rate jump tests for determining the local strain-rate sensitivity in nanocrystalline Ni and ultrafine-grained Al. *J. Mater. Res.* **26**, 1421 (2011).
13. V. Maier, B. Merle, M. Göken, and K. Durst: An improved long-term nanoindentation creep testing approach for studying the local deformation processes in nanocrystalline metals at room and elevated temperatures. *J. Mater. Res.* **28**, 1177 (2013).
14. R. Pippan, S. Scheriau, A. Hohenwarter, and M. Hafok: Advantages and limitations of HPT: A review. *Mater. Sci. Forum* **584–586**, 16 (2008).
15. K. Edalati and Z. Horita: A review on high-pressure torsion (HPT) from 1935 to 1988. *Mater. Sci. Eng., A* **652**, 325 (2016).
16. X.H. An, S. Qu, S.D. Wu, and Z.F. Zhang: Effects of stacking fault energy on the thermal stability and mechanical properties of nanostructured Cu–Al alloys during thermal annealing. *J. Mater. Res.* **26**, 407 (2011).
17. X.H. An, S.D. Wu, and Z.F. Zhang: Influence of stacking fault energy on the microstructures and grain refinement in the Cu–Al alloys during equal-channel angular pressing. *Mater. Sci. Forum* **667–669**, 379 (2011).
18. X.H. An, S.D. Wu, Z.F. Zhang, R.B. Figueiredo, N. Gao, and T.G. Langdon: Evolution of microstructural homogeneity in copper processed by high-pressure torsion. *Scr. Mater.* **63**, 560 (2010).
19. X.H. An, Q.Y. Lin, S.D. Wu, Z.F. Zhang, R.B. Figueiredo, N. Gao, and T.G. Langdon: Formation of fivefold deformation twins in an ultrafine-grained copper alloy processed by high-pressure torsion. *Scr. Mater.* **64**, 249 (2011).
20. X.H. An, W.Z. Han, C.X. Huang, P. Zhang, G. Yang, S.D. Wu, and Z.F. Zhang: High strength and utilizable ductility of bulk ultrafine-grained Cu–Al alloys. *Appl. Phys. Lett.* **92**, 23 (2008).
21. W.Z. Han, Z.F. Zhang, S.D. Wu, and S.X. Li: Combined effects of crystallographic orientation, stacking fault energy and grain size on deformation twinning in fcc crystals. *Philos. Mag.* **88**, 3011 (2008).
22. Y.L. Gong, C.E. Wen, X.X. Wu, S.Y. Ren, L.P. Cheng, and X.K. Zhu: The influence of strain rate, deformation temperature and stacking fault energy on the mechanical properties of Cu alloys. *Mater. Sci. Eng., A* **583**, 199 (2013).
23. Y. Zhang, N.R. Tao, and K. Lu: Effects of stacking fault energy, strain rate and temperature on the microstructure and strength of nanostructured Cu–Al alloys subjected to plastic deformation. *Acta Mater.* **59**, 6048 (2011).
24. M. Hafok and R. Pippan: Influence of stacking fault energy and alloying on stage V hardening of HPT-deformed materials. *Int. J. Mater. Res.* **101**, 1097 (2010).
25. K. Edalati, D. Akama, A. Nishio, S. Lee, Y. Yonenaga, J.M. Cubero-Sesin, and Z. Horita: Influence of dislocation–solute atom interactions and stacking fault energy on grain size of single-phase alloys after severe plastic deformation using high-pressure torsion. *Acta Mater.* **69**, 68 (2014).
26. A. Hohenwarter, A. Taylor, R. Stock, and R. Pippan: Effect of large shear deformations on the fracture behavior of a fully pearlitic steel. *Metallurgical and Materials Transactions A* **42**, 1609 (2011).
27. X. An, Q. Lin, S. Wu, and Z. Zhang: Improved fatigue strengths of nanocrystalline Cu and Cu–Al alloys. *Mater. Res. Lett.* **3**, 135 (2015).
28. P.C.J. Gallagher: The influence of alloying, temperature, and related effects on the stacking fault energy. *Metall. Trans.* **1**, 2429 (1970).
29. O. Engler: Deformation and texture of copper–manganese alloys. *Acta Mater.* **48**, 4827 (2000).
30. W.C. Oliver and G.M. Pharr: Improved technique for determining hardness and elastic modulus using load and displacement sensing indentation experiments. *J. Mater. Res.* **7**, 1564 (1992).
31. K. Durst and V. Maier: Dynamic nanoindentation testing for studying thermally activated processes from single to nanocrystalline metals. *Curr. Opin. Solid State Mater. Sci.* **19**, 340 (2015).
32. G.M. Pharr, J.H. Strader, and W.C. Oliver: Critical issues in making small-depth mechanical property measurements by nanoindentation with continuous stiffness measurement. *J. Mater. Res.* **24**, 653 (2009).
33. B. Merle, V. Maier-Kiener, and G.M. Pharr: Influence of modulus-to-hardness ratio and harmonic parameters on continuous stiffness measurement during nanoindentation. *Acta Mater.* **134**, 167 (2017).
34. B.N. Lucas and W.C. Oliver: Indentation power-law creep of high-purity indium. *Metall. Mater. Trans. A* **30**, 601 (1999).

https://doi.org/10.1557/jmr.2017.320 Published online by Cambridge University Press

35. V. Maier, C. Schunk, M. Göken, and K. Durst: Microstructure-dependent deformation behaviour of bcc-metals—Indentation size effect and strain rate sensitivity. *Philos. Mag.* **95**, 1766 (2014).
36. Q. Wei, S. Cheng, K.T. Ramesh, and E. Ma: Effect of nanocrystalline and ultrafine grain sizes on the strain rate sensitivity and activation volume: Fcc versus bcc metals. *Mater. Sci. Eng., A* **381**, 71 (2004).
37. K. Durst, B. Backes, and M. Göken: Indentation size effect in metallic materials: Correcting for the size of the plastic zone. *Scr. Mater.* **52**, 1093 (2005).
38. M. Rester, C. Motz, and R. Pippan: Stacking fault energy and indentation size effect: DO they interact? *Scr. Mater.* **58**, 187 (2008).
39. A.A. Elmustafa and D.S. Stone: Stacking fault energy and dynamic recovery: Do they impact the indentation size effect? *Mater. Sci. Eng., A* **358**, 1 (2003).
40. A. Portevin and H. Le Chatelier: Heat treatment of aluminium-copper alloys. *Trans. Am. Soc. Steel Treat.* **5**, 457 (1924).
41. W. Blum and X.H. Zeng: A simple dislocation model of deformation resistance of ultrafine-grained materials explaining Hall–Petch strengthening and enhanced strain rate sensitivity. *Acta Mater.* **57**, 1966 (2009).
42. N. Ahmed and A. Hartmaier: Mechanisms of grain boundary softening and strain-rate sensitivity in deformation of ultrafine-grained metals at high temperatures. *Acta Mater.* **59**, 4323 (2011).
43. X.X. Wu, X.Y. San, Y.L. Gong, L.P. Chen, C.J. Li, and X.K. Zhu: Studies on strength and ductility of Cu–Zn alloys by stress relaxation. *Mater. Des.* **47**, 295 (2013).
44. W. Blum, Y.J. Li, and K. Durst: Stability of ultrafine-grained Cu to subgrain coarsening and recrystallization in annealing and deformation at elevated temperatures. *Acta Mater.* **57**(17), 5207–5217 (2009).

https://doi.org/10.1557/jmr.2017.320 Published online by Cambridge University Press